

P. COLLI FRANZONE P. DEUFLHARD B. ERDMANN
J. LANG L. F. PAVARINO

**Adaptivity in Space and Time for
Reaction-Diffusion Systems in
Electrocardiology**

Adaptivity in Space and Time for Reaction-Diffusion Systems in Electrocardiology

Piero Colli Franzone¹ Peter Deuffhard² Bodo Erdmann²
Jens Lang³ Luca F. Pavarino⁴

Abstract

Adaptive numerical methods in space and time are introduced and studied for multiscale cardiac reaction-diffusion models in three dimensions. The evolution of a complete heartbeat, from the excitation to the recovery phase, is simulated with both the anisotropic Bidomain and Monodomain models, coupled with either a variant of the simple FitzHugh-Nagumo model or the more complex phase-I Luo-Rudy ionic model. The simulations are performed with the KARDOS library, that employs adaptive finite elements in space and adaptive linearly implicit methods in time. The numerical results show that this adaptive method successfully solves these complex cardiac reaction-diffusion models on three-dimensional domains of moderate sizes. By automatically adapting the spatial meshes and time steps to the proper scales in each phase of the heartbeat, the method accurately resolves the evolution of the intra- and extra-cellular potentials, gating variables and ion concentrations during the excitation, plateau and recovery phases.

Keywords: reaction-diffusion equations, cardiac Bidomain and Monodomain models, adaptive finite elements, adaptive time integration

1 Introduction

Recent advances in contemporary cardiac electrophysiology are progressively revealing the complex multiscale structure of the bioelectrical activity of the

¹Dipartimento di Matematica, Università di Pavia, Via Ferrata 1, 27100 Pavia, Italy. E-mail: colli@imati.cnr.it

²Zuse Institute Berlin, Takustr. 7, 14195 Berlin-Dahlem, Germany. E-mail: {deuffhard, erdmann}@zib.de

³Technische Universität Darmstadt, Schlossgartenstr. 7, 64289 Darmstadt, Germany. E-mail: lang@mathematik.tu-darmstadt.de

⁴Dipartimento di Matematica, Università di Milano, Via Saldini 50, 20133 Milano, Italy. E-mail: pavarino@mat.unimi.it

heart, from the microscopic activity of ion channels of the cellular membrane to the macroscopic properties of the anisotropic propagation of excitation and recovery fronts in the whole heart; see e.g. ZIPES and JALIFE [67], KLEBER and RUDY [34], PANFILOV and HOLDEN [45]. The experimental study of these complex phenomena has been increasingly coupled with multiscale modeling and simulations, including more detailed features of each component in more refined mathematical models with appropriate space and time scales. The most complete of these models describe the cardiac tissue by a reaction-diffusion system of partial differential equations (the Bidomain model), coupled with a system of ordinary differential equations (e.g. Luo-Rudy ionic models) describing the ionic currents associated with the reaction terms. These models can be computationally very expensive because of the different space and time scales involved. We recall here that meaningful portions of cardiac tissue have sizes on the order of centimeters, while the steep excitation front requires discretizations on the order of a tenth of millimeter. Moreover, while a normal heartbeat is on the order of one second, the time constants of the rapid kinetics involved range from 0.1 to 500 milliseconds, requiring in some phases time steps on the order of the hundredths of milliseconds (or less when currents or shocks are applied). Hence, realistic three-dimensional models employing uniform grids can yield discrete problems with more than $O(10^7)$ unknowns at every time step and simulations can run for many thousands of time steps; see COLLI FRANZONE and PAVARINO [13, 46, 14] for some large scale parallel simulations.

In order to overcome these computational limits, in this paper we introduce and study an adaptive numerical method in both space and time for cardiac reaction-diffusion models in three dimensions. We consider both the anisotropic Bidomain and Monodomain models, coupled with either a variant of the simple FitzHugh-Nagumo model or the more complex phase-I Luo-Rudy ionic model. We simulate the evolution of a complete heartbeat, from the excitation (depolarization) phase to the following plateau and recovery (repolarization) phases. Our simulations are performed with the KARDOS library [21, 1], that employs adaptive finite elements in space and adaptive linearly implicit methods in time. The results presented in this paper show that our adaptive method can successfully solve these complex cardiac reaction-diffusion models on three-dimensional domains of moderate sizes, but further research is needed in order to extend the simulations to larger and more realistic cardiac domains. For previous work on adaptive methods for parabolic reaction-diffusion systems in two dimensions, see CHERRY et al. [9], YU [66], TRANGENSTEIN [61], while see MOORE [42] for an alternative adaptive method in three dimensions.

We remark that most simulations in computational electrocardiology are based on the simpler Monodomain model, while in this paper we also consider the full Bidomain system in three dimensions. The few other Bidomain simulations present in the literature often employ some simplifications of the model, such as two-dimensional domains, simpler ionic models, operator splitting of the elliptic-parabolic formulation of the Bidomain system, coarser time or space mesh size for the elliptic subproblem, etc.; see COLLI FRANZONE ET AL. [10, 11], ROTH [52, 53, 54], HOOKE et al. [31], PORMANN [48], HENRIQUEZ et al. [28, 29, 44], VIGMOND et al. [64], SAMBELASHVILI and EFIMOV [55], ASHIHARA et al. [3], DOS SANTOS et al. [65], MURILLO and CAI [43], PENNACCHIO and SIMONCINI [47], SUNDNES et al. [58].

The rest of the paper is organized as follows. In Section 2, we introduce the standard model of cardiac tissue including its fiber structure and conductivity tensors (2.1), the anisotropic Bidomain model for the intra- and extra-cellular potentials (2.2) and the simpler anisotropic Monodomain model (2.3). In Section 3, the basic ideas of cellular ionic models of Hodgkin-Huxley type are reviewed, focusing on a FitzHugh-Nagumo variant (3.1) and the phase-I Luo-Rudy model (3.2) that will be employed in our cardiac model. In Section 4, we describe the adaptive numerical discretization of our models using the KARDOS library, focusing on the adaptive time discretization by linearly implicit methods (4.1) and the multilevel finite elements employed in the adaptive space discretization (4.2). Finally, in Section 5 we present the results of several numerical experiments in three dimensions.

2 Cardiac reaction-diffusion models

2.1 Cardiac fibers and conductivity tensors

The cardiac ventricular tissue can be modeled as an arrangement of cardiac fibers which rotate counterclockwise from epi- to endocardium (STREETER [59]) and which has a laminar organization modeled as a set of muscle sheets running radially from epi- to endocardium (LEGRICE ET AL. [39]). Therefore, at every point \mathbf{x} it is possible to identify a triplet of orthonormal principal axes $\mathbf{a}_l(\mathbf{x})$, $\mathbf{a}_t(\mathbf{x})$, $\mathbf{a}_n(\mathbf{x})$, with $\mathbf{a}_l(\mathbf{x})$ parallel to the local fiber direction, $\mathbf{a}_t(\mathbf{x})$ and $\mathbf{a}_n(\mathbf{x})$ tangent and orthogonal to the radial laminae, respectively, and both being transversal to the fiber axis. The macroscopic Bidomain model represents the cardiac tissue as the superposition of two anisotropic continuous media, the intra- (i) and extra- (e) cellular media, coexisting at every point of the tissue and separated by a distributed continuous cellular membrane; see e.g. HENRIQUEZ [28] and KEENER and SNEYD [33].

Denoting by $\sigma_l^{i,e}$, $\sigma_t^{i,e}$, $\sigma_n^{i,e}$ the conductivity coefficients in the intra- and extra-cellular media measured along the corresponding directions $\mathbf{a}_l, \mathbf{a}_t, \mathbf{a}_n$, then the anisotropic conductivity tensors $D_i(\mathbf{x})$ and $D_e(\mathbf{x})$ related to *orthotropic anisotropy* of the media are given by:

$$D_{i,e}(\mathbf{x}) = \sigma_l^{i,e} \mathbf{a}_l(\mathbf{x}) \mathbf{a}_l^T(\mathbf{x}) + \sigma_t^{i,e} \mathbf{a}_t(\mathbf{x}) \mathbf{a}_t^T(\mathbf{x}) + \sigma_n^{i,e} \mathbf{a}_n(\mathbf{x}) \mathbf{a}_n^T(\mathbf{x}). \quad (1)$$

For *axisymmetric* anisotropic media, $\sigma_n^{i,e} = \sigma_t^{i,e}$, we have

$$D_{i,e}(\mathbf{x}) = \sigma_t^{i,e} I + (\sigma_l^{i,e} - \sigma_t^{i,e}) \mathbf{a}_l(\mathbf{x}) \mathbf{a}_l^T(\mathbf{x}).$$

2.2 The anisotropic Bidomain model

The intra- and extra-cellular electric potentials u_i, u_e in the anisotropic Bidomain model are described by a reaction-diffusion system coupled with a system of ODEs for ionic gating variables w and for the ion concentrations c . We denote by $v = u_i - u_e$ the transmembrane potential and by

$$I_m = c_m \frac{\partial v}{\partial t} + I_{ion}(v, w, c)$$

the membrane current per unit volume, where $c_m = \chi * C_m$, $I_{ion} = \chi * i_{ion}$, with χ the ratio of membrane area per tissue volume, C_m the surface capacitance and i_{ion} the ionic current of the membrane per unit area. Let I_{app}^e be an applied extra-cellular current per unit volume, satisfying the compatibility condition $\int_{\Omega} I_{app}^e dx = 0$, and $\mathbf{j}_{i,e} = -D_{i,e} \nabla u_{i,e}$ the intra- and extra-cellular current density. Due to the current conservation law, we have

$$\operatorname{div} \mathbf{j}_i = -I_m, \quad \operatorname{div} \mathbf{j}_e = I_m - I_{app}^e.$$

Then the anisotropic Bidomain model in the unknown potentials $(u_i(\mathbf{x}, t), u_e(\mathbf{x}, t))$, $v(\mathbf{x}, t) = u_i(\mathbf{x}, t) - u_e(\mathbf{x}, t)$, gating variables $w(\mathbf{x}, t)$ and ion concentrations $c(\mathbf{x}, t)$ can be written as:

$$\begin{aligned} c_m \partial_t v - \operatorname{div}(D_i \nabla u_i) + I_{ion}(v, w, c) &= 0 & \text{in } \Omega \times (0, T) \\ -c_m \partial_t v - \operatorname{div}(D_e \nabla u_e) - I_{ion}(v, w, c) &= -I_{app}^e & \text{in } \Omega \times (0, T) \\ \partial_t w - R(v, w) &= 0, \quad \partial_t c - S(v, w, c) &= 0 & \text{in } \Omega \times (0, T) \\ \mathbf{n}^T D_{i,e} \nabla u_{i,e} &= 0 & \text{in } \partial\Omega \times (0, T) \\ v(\mathbf{x}, 0) &= v_0(\mathbf{x}), \quad w(\mathbf{x}, 0) = w_0(\mathbf{x}), \quad c(\mathbf{x}, 0) = c_0(\mathbf{x}) & \text{in } \Omega, \end{aligned} \quad (2)$$

where we have imposed insulated boundary conditions. The system uniquely determines v , while the potentials u_i and u_e are defined only up to a same

additive time-dependent constant relating to the reference potential. This potential is chosen to be the average extra-cellular potential in the cardiac volume by imposing $\int_{\Omega} u_e \, dx = 0$. We refer to [12] for a mathematical analysis of the Bidomain model. In the following, we will consider as ionic membrane models some Luo-Rudy models which are briefly recalled in Section 3; (see LUO and RUDY [41]). These models specify the reaction term I_{ion} and the functions $R(v, w)$ and $S(v, w, c)$ determining the evolution of the gating variables w and the ions concentrations c .

In terms of the transmembrane and extra-cellular potentials $v(\mathbf{x}, t)$ and $u_e(\mathbf{x}, t)$, we obtain the following equivalent formulation of the reaction-diffusion equations of the anisotropic Bidomain Model:

$$\begin{aligned} c_m \partial_t v + I_{ion}(v, w, c) + \operatorname{div}(D_e \nabla u_e) &= I_{app}^e \quad \text{in } \Omega \times (0, T) \\ -\operatorname{div}((D_i + D_e) \nabla u_e) &= \operatorname{div}(D_i \nabla v) - I_{app}^e \quad \text{in } \Omega \times (0, T). \end{aligned} \quad (3)$$

2.3 The simplified anisotropic Monodomain model

It is well known that the Bidomain system reduces to the Monodomain model if we assume equal anisotropy ratio of the two media. We shall mention here another interesting derivation of a reduced Bidomain model which does not make such an assumption and that we will still call Monodomain model. Denoting by $J_{tot} = \mathbf{j}_i + \mathbf{j}_e$ the total current flowing in the two media, since $J_{tot} = -D_i \nabla u_i - D_e \nabla u_e$, substituting $u_i = v + u_e$, we get

$$\nabla u_e = -D^{-1} D_i \nabla v - D^{-1} J_{tot}, \quad (4)$$

with $D = D_i + D_e$. Therefore, the second equation in the Bidomain system can be written as

$$-c_m \partial_t v + \operatorname{div}(D_e D^{-1} D_i \nabla v) + \operatorname{div}(D_e D^{-1} J_{tot}) - I_{ion}(v, w) = -I_{app}^e. \quad (5)$$

Since the tensors (1) can be written as

$$D_{i,e}(\mathbf{x}) = \sigma_l^{i,e} I + (\sigma_t^{i,e} - \sigma_l^{i,e}) \mathbf{a}_t(\mathbf{x}) \mathbf{a}_t^T(\mathbf{x}) + (\sigma_n^{i,e} - \sigma_l^{i,e}) \mathbf{a}_n(\mathbf{x}) \mathbf{a}_n^T(\mathbf{x}),$$

then

$$D_e D^{-1} = \mu_l^e I + (\mu_t^e - \mu_l^e) \mathbf{a}_t(\mathbf{x}) \mathbf{a}_t^T(\mathbf{x}) + (\mu_n^e - \mu_l^e) \mathbf{a}_n(\mathbf{x}) \mathbf{a}_n^T(\mathbf{x}), \quad (6)$$

with $\mu_{l,t,n}^e = \sigma_{l,t,n}^e / (\sigma_{l,t,n}^e + \sigma_{l,t,n}^i)$. Assuming constant conductivity coefficients and taking into account that $\text{div } J_{tot} = -I_{app}^e$, we have

$$\begin{aligned} \text{div}(D_e D^{-1} J_{tot}) &= \mu_l^e \text{div } J_{tot} + (\mu_t^e - \mu_l^e) \text{div}(\mathbf{a}_t(\mathbf{x}) \mathbf{a}_t^T(\mathbf{x}) J_{tot}) \\ &\quad + (\mu_n^e - \mu_l^e) \text{div}(\mathbf{a}_n(\mathbf{x}) \mathbf{a}_n^T(\mathbf{x}) J_{tot}) \\ &= -\mu_l^e I_{app}^e + (\mu_t^e - \mu_l^e) \text{div}(\mathbf{a}_t(\mathbf{x}) \mathbf{a}_t^T(\mathbf{x}) J_{tot}) \\ &\quad + (\mu_n^e - \mu_l^e) \text{div}(\mathbf{a}_n(\mathbf{x}) \mathbf{a}_n^T(\mathbf{x}) J_{tot}). \end{aligned} \quad (7)$$

From (4) it follows $-D_e D^{-1} D_i \nabla v = D_e D^{-1} J_{tot} + D_e \nabla u_e$, hence the flux relationship

$$\mathbf{n}^T D_e D^{-1} D_i \nabla v = \mathbf{n}^T D_e D^{-1} J_{tot} + \mathbf{n}^T D_e \nabla u_e. \quad (8)$$

Using (6), the first term on the right-hand side can be written as

$$\mathbf{n}^T (D_e D^{-1} J_{tot}) = \mu_l^e \mathbf{n}^T J_{tot} + (\mu_t^e - \mu_l^e) (\mathbf{n}^T \mathbf{a}_t) (\mathbf{a}_t^T J_{tot}) + (\mu_n^e - \mu_l^e) (\mathbf{n}^T \mathbf{a}_n) (\mathbf{a}_n^T J_{tot}).$$

The insulating conditions $\mathbf{n}^T \mathbf{j}_i = \mathbf{n}^T \mathbf{j}_e = 0$ imply $\mathbf{n}^T J_{tot} = 0$, i.e., J_{tot} is tangent to $\partial\Omega$, and assuming that the fibers are also tangent to $\partial\Omega$, we have $\mathbf{n}^T \mathbf{a}_\nu = 0$ and $\mathbf{a}_t^T J_{tot} = 0$. Substituting these conditions in (8) it follows the Monodomain boundary condition

$$\mathbf{n}^T D_e D^{-1} D_i \nabla v = 0. \quad (9)$$

Disregarding the two additional terms in (7) related to the projections of J_{tot} on the directions across fiber \mathbf{a}_t and \mathbf{a}_n (which disappear for media having equal anisotropic ratio $\mu_l^e = \mu_t^e = \mu_n^e$), it results $\text{div}(D_e D^{-1} J_{tot}) \approx -\mu_l^e I_{app}^e$. Substituting this approximation in (5) and considering the boundary condition (9), we obtain the anisotropic Monodomain model consisting in a single parabolic reaction-diffusion equation for v with the conductivity tensor $D_m = D_e D^{-1} D_i$, $I_{app}^m = -I_{app}^e \sigma_l^i / (\sigma_l^e + \sigma_l^i)$ and coupled with the same gating system

$$\begin{aligned} c_m \partial_t v - \text{div}(D_m \nabla v) + I_{ion}(v, w, c) &= I_{app}^m && \text{in } \Omega \times (0, T) \\ \partial_t w - R(v, w) = 0, \quad \partial_t c - S(v, w, c) &= 0 && \text{in } \Omega \times (0, T) \\ \mathbf{n}^T D_m \nabla v &= 0 && \text{in } \partial\Omega \times (0, T) \\ v(\mathbf{x}, 0) = v_0(\mathbf{x}), \quad w(\mathbf{x}, 0) = w_0(\mathbf{x}), \quad c(\mathbf{x}, 0) = c_0(\mathbf{x}) &&& \text{in } \Omega. \end{aligned} \quad (10)$$

From the knowledge of the distribution of $v(\mathbf{x}, t)$ the extra-cellular potential distribution u_e is derived by solving the elliptic boundary value problem

$$-\text{div}(D \nabla u_e) = \text{div}(D_i \nabla v), \quad -\mathbf{n}^T D \nabla u_e = \mathbf{n}^T D_i \nabla v.$$

3 Membrane models and ionic currents

Following the celebrated work by HODGKIN and HUXLEY [30] (1963 Medicine Nobel prize) on nerve action potential, many models of Hodgkin-Huxley type have later been developed for the cardiac action potential. In these models, the ionic current through channels of the membrane, due to the transmembrane potential v , M gating and Q ionic concentration variables $w := (w_1, \dots, w_M)$, $c := (c_1, \dots, c_Q)$, is given by

$$I_{ion}(v, w, c) = \sum_{k=1}^N G_k(v) \prod_{j=1}^M w_j^{p_{jk}} (v - v_k(c)),$$

where $G_k(v)$ is the membrane conductance, v_k is the Nerst equilibrium potential for the k -th current and p_{jk} are integers. The dynamics of the gating and concentration variables is described by a system of ordinary differential equations which when w_j is a gating variable ($0 \leq w_j \leq 1$) have the form

$$\partial_t w_j = \alpha_j(v)(1 - w_j) - \beta_j(v)(w_j), \quad (11)$$

with coefficients $\alpha_j > 0$, $\beta_j > 0$, and appropriate initial conditions.

Many refinements of the original Hodgkin-Huxley model have been proposed by fitting improved experimental data with more complex models; for example, we recall here the models by Beeler-Reuter (1977, $N = 4$, $M = 7$), phase-I Luo-Rudy (1991, $N = 6$, $M = 7$), phase-II Luo-Rudy (1994, $N = 10$, $M = 7$); see HUND and RUDY [32] for current developments.

3.1 A FitzHugh-Nagumo variant

Simplified models of lower complexity (with 1 or 2 gating variables) have been proposed too. The simplest and most used is the FitzHugh-Nagumo (FHN) model ($N = 1$, $M = 1$), that yields only a coarse approximation of a typical cardiac action potential, particularly in the plateau and repolarization phases. A better approximation is given by the following FHN variant by Rogers and McCulloch[50]

$$\begin{aligned} I_{ion}(v, w) &= Gv \left(1 - \frac{v}{v_{th}}\right) \left(1 - \frac{v}{v_p}\right) + \eta_1 vw, \\ \frac{\partial w}{\partial t} &= \eta_2 \left(\frac{v}{v_p} - \eta_3 w\right), \end{aligned}$$

where $G, \eta_1, \eta_2, \eta_3$ are positive real coefficients, v_{th} is a threshold potential and v_p the peak potential. The gating variable w satisfies

$$\partial_t w = \eta v - \gamma w,$$

with $\eta, \gamma > 0$. We will consider this FHN variant as our simplest gating model.

3.2 The LR1 ionic model

In this paper, we will also consider the more detailed phase-I Luo-Rudy (LR1) model (see [41]), where I_{ion} is the sum of $N = 6$ currents

$$I_{ion} = I_{Na} + I_{si} + I_K + I_{K1} + I_{Kp} + I_b,$$

two inwards (I_{Na} and I_{si}) and four outwards (I_K, I_{K1}, I_{Kp}, I_b). The first three currents depend on six gating variables and one ion (calcium) concentration, while the last three are time-independent.

The fast sodium current I_{Na} is given by

$$I_{Na} = g_{Na} m^3 h j (v - v_{Na}),$$

where $g_{Na} = 23 \text{ mS/cm}^2$, $v_{Na} = 54.4 \text{ mV}$, and the gating variables h, j, m satisfy ordinary differential equations (11) with coefficients

$$\alpha_h = \begin{cases} 0 & v \geq -40 \\ 0.135 \exp\left(\frac{80+v}{-6.8}\right) & v < -40, \end{cases}$$

$$\beta_h = \begin{cases} 0.13(1 + \exp\left(\frac{10.66+v}{-11.1}\right)) & v \geq -40 \\ 3.56 \exp(0.079 v) + 3.1 \cdot 10^5 \exp(0.35 v) & v < -40, \end{cases}$$

$$\alpha_j = \begin{cases} 0 & v \geq -40 \\ -1.2714 \cdot 10^5 \exp(0.2444 v) - 3.474 \cdot 10^5 \exp(-0.04391 v) & v < -40, \end{cases}$$

$$\beta_j = \begin{cases} 0.3 \frac{\exp(-2.535 \cdot 10^{-7} v)}{1 + \exp(-0.1(32+v))} & v \geq -40 \\ 0.1212 \frac{\exp(-0.01052 v)}{1 + \exp(-0.1378(40.14+v))} & v < -40, \end{cases}$$

$$\alpha_m = 0.32 \frac{47.13 + v}{1 - \exp(-47.13 - v)}, \quad \beta_m = 0.08 \exp\left(\frac{-v}{11}\right).$$

The slow inward current I_{si} is given by

$$I_{si} = g_{si} d f (v - v_{si}),$$

where $g_{si} = 0.09 \text{ mS/cm}^2$, $v_{si} = 7.7 - 13.0287 \log([Ca]_i)$, $[Ca]_i$ is the calcium ion concentration satisfying a special ordinary differential equation

$$d[Ca]_i/dt = 0.07(10^{-4} - [Ca]_i) - 10^{-4}I_{si}$$

and the gating variables d, f satisfy equations (11) with coefficients

$$\begin{aligned} \alpha_d &= 0.095 \frac{\exp(-0.01(v - 5))}{1 + \exp(-0.072(v - 5))}, & \beta_d &= 0.07 \frac{\exp(-0.017(v + 44))}{1 + \exp(0.05(v + 44))}, \\ \alpha_f &= 0.012 \frac{\exp(-0.008(v + 28))}{1 + \exp(0.15(v + 28))}, & \beta_f &= 0.0065 \frac{\exp(-0.02(v + 30))}{1 + \exp(-0.2(v + 30))}. \end{aligned}$$

The time-dependent potassium current I_K is given by

$$I_K = g_K X X_i (v - v_K),$$

where $g_K = 0.282 \text{ mS/cm}^2$, $v_K = -77 \text{ mV}$, X is a gating variable satisfying (11) with coefficients

$$\alpha_X = 0.0005 \frac{\exp(0.083(v + 50))}{1 + \exp(0.057(v + 50))}, \quad \beta_X = 0.0013 \frac{\exp(-0.06(v + 20))}{1 + \exp(-0.04(v + 20))},$$

and X_i is an additional variable given by

$$X_i = \begin{cases} 2.837 \frac{\exp(0.04(v + 77)) - 1}{(v + 77) \exp(0.04(v + 35))} & v > -100 \\ 1 & v \leq -100. \end{cases}$$

The time-independent potassium current I_{K1} is given by

$$I_{K1} = g_{K1} K1_\infty (v - v_{K1}),$$

where $g_{K1} = 0.6047 \sqrt{[K]_o/5.4}$, $v_{K1} = v_{Na} \log([K]_o/[K]_i) / \log([Na]_o/[Na]_i)$, with the constant ion concentrations $[K]_o = 5.4$, $[K]_i = 145$, $[Na]_o = 140$, $[Na]_i = 18$ (all in mM), and $K1_\infty = \alpha_{K1}/(\alpha_{K1} + \beta_{K1})$, with

$$\begin{aligned} \alpha_{K1} &= \frac{1.02}{1 + \exp(0.2385(v - v_{K1} - 59.215))}, \\ \beta_{K1} &= \frac{0.49124 \exp(0.08032(v - v_{K1} + 5.476)) + \exp(0.06175(v - v_{K1} - 594.31))}{1 + \exp(-0.5143(v - v_{K1} + 4.753))}. \end{aligned}$$

The plateau potassium current I_{Kp} is given by

$$I_{Kp} = g_{Kp} K_p (v - v_{Kp}),$$

where $g_{Kp} = 0.0183 \text{ mS/cm}^2$, $v_{Kp} = v_{K1}$ and $K_p = 1/(1 + \exp((7.488 - v)/5.98))$.

The background current I_b is given by

$$I_b = g_b (v - v_b),$$

where $g_b = 0.03921 \text{ mS/cm}^2$ and $v_b = -59.87 \text{ mV}$.

4 Adaptive numerical discretization and the KARDOS library

The anisotropic Monodomain (10) and Bidomain models (2) are discretized by linearly implicit methods in time and adaptive finite elements in space, using the KARDOS library [21, 1].

One of the important requirements that modern software must meet today is to judge the quality of its numerical approximations in order to assess safely the modelling process. Adaptive methods have proven to work efficiently providing a posteriori error estimates and appropriate strategies to improve the accuracy where needed. They are now entering into real-life applications and starting to become a standard feature in simulation programs. The present paper reports on one successful way to construct discretization methods adaptive in space and time, which are applicable to a wide range of practically relevant problems.

We concentrate on reaction–diffusion problems which can be written in the form

$$B(x, t, u, \nabla u) \partial_t u = \nabla \cdot (D(x, t, u, \nabla u) \nabla u) + F(x, t, u, \nabla u), \quad (12)$$

supplemented with suitable boundary and initial conditions. The vector-valued solution $u = (u_1, \dots, u_m)^T$ is supposed to be unique.

In the classical method of lines (MOL) approach, the spatial discretization is done once and kept fixed during the time integration. Here, we allow a local spatial refinement in each time step, which results in a discretization sequence first in time then in space. The spatial discretization is considered as a perturbation, which has to be controlled within each time

step. Combined with a posteriori error estimates this approach is known as adaptive Rothe method. First theoretical investigations have been made by BORNEMANN [7] for linear parabolic equations. LANG and WALTER [38] have generalized the adaptive Rothe approach to reaction–diffusion systems. A rigorous analysis for nonlinear parabolic systems is given in LANG [36]. For a comparative study, we refer to DEUFLHARD, LANG, and NOWAK [20].

Since differential operators give rise to infinite stiffness, often an implicit method is applied to discretize in time. We use linearly implicit methods of Rosenbrock type, which are constructed by incorporating the Jacobian directly into the formula. These methods offer several advantages. They completely avoid the solution of nonlinear equations, that means no Newton iteration has to be controlled. There is no problem to construct Rosenbrock methods with optimum linear stability properties for stiff equations. According to their one–step nature, they allow a rapid change of step sizes and an efficient adaptation of the spatial discretization in each time step. Moreover, a simple embedding technique can be used to estimate the error in time satisfactorily. A description of the main idea of linearly implicit methods is given in Subsection 4.1.

Linear finite elements are used for the spatial discretization. To estimate the error in space, the hierarchical basis technique has been extended to Rosenbrock schemes in LANG [36]. Hierarchical error estimators have been accepted to provide efficient and reliable assessment of spatial errors. They can be used to steer a multilevel process, which aims at getting a successively improved spatial discretization drastically reducing the size of the arising linear algebraic systems with respect to a prescribed tolerance (BORNEMANN, ERDMANN, and KORNUBER [8], DEUFLHARD, LEINEN and YSERENTANT [19], BANK and SMITH [4]). A brief introduction to multilevel finite element methods is given in Subsection 4.2.

The described algorithm has been coded in the fully adaptive software package KARDOS at the Konrad–Zuse–Zentrum in Berlin. Several types of embedded Rosenbrock solvers and adaptive finite elements were implemented. KARDOS is based on the KASKADE–toolbox [22]. Nowadays both codes are efficient and reliable workhorses to solve a wide class of PDEs in one, two, or three space dimensions.

4.1 Linearly implicit methods

In this section a short description of the linearly implicit discretization idea is given. More details can be found in the books of HAIRER and WANNER [27], DEUFLHARD and BORNEMANN [18], STREHMEL and WEINER [57]. For

ease of presentation, we firstly set $B = I$ in (12) and consider the autonomous case. Then we can look at (12) as an abstract Cauchy problem of the form

$$\partial_t u = f(u), \quad u(t_0) = u_0, \quad t > t_0, \quad (13)$$

where the differential operators and the boundary conditions are incorporated into the nonlinear function $f(u)$. Since differential operators give rise to infinite stiffness, often an implicit discretization method is applied to integrate in time. The simplest scheme is the implicit (backward) Euler method

$$u_{n+1} = u_n + \tau f(u_{n+1}), \quad (14)$$

where $\tau = t_{n+1} - t_n$ is the step size and u_n denotes an approximation of $u(t)$ at $t = t_n$. This equation is implicit in u_{n+1} and thus usually a Newton-like iteration method has to be used to approximate the numerical solution itself. The implementation of an efficient nonlinear solver is the main problem for a fully implicit method.

Investigating the convergence of Newton's method in function space, DEUFLHARD [16] pointed out that one calculation of the Jacobian or an approximation of it per time step is sufficient to integrate stiff problems efficiently. Using u_n as an initial iterate in a Newton method applied to (14), we find

$$(I - \tau J_n) K_n = \tau f(u_n), \quad (15)$$

$$u_{n+1} = u_n + K_n, \quad (16)$$

where J_n stands for the Jacobian matrix $\partial_u f(u_n)$. The arising scheme is known as the *linearly implicit* Euler method. The numerical solution is now effectively computed by solving the system of linear equations that defines the increment K_n . Among the methods which are capable of integrating stiff equations efficiently, the linearly implicit methods are the easiest to program, since they completely avoid the numerical solution of nonlinear systems.

One important class of higher-order linearly implicit methods consists of extrapolation methods that are very effective in reducing the error, see DEUFLHARD [17]. However, in the case of higher spatial dimension, several drawbacks of extrapolation methods have shown up in numerical experiments made by BORNEMANN [6]. Another generalization of the linearly implicit approach we will follow here leads to Rosenbrock methods (ROSEN-BROCK [51]). They have found wide-spread use in the ODE context. Applied

to (13) a so-called s -stage Rosenbrock method has the recursive form

$$(I - \tau \gamma_{ii} J_n) K_{ni} = \tau f(u_n + \sum_{j=1}^{i-1} \alpha_{ij} K_{nj}) + \tau J_n \sum_{j=1}^{i-1} \gamma_{ij} K_{nj}, \quad i = 1(1)s, \quad (17)$$

$$u_{n+1} = u_n + \sum_{i=1}^s b_i K_{ni}, \quad (18)$$

where the step number s and the defining formula coefficients b_i , α_{ij} , and γ_{ij} are chosen to obtain a desired order of consistency and good stability properties for stiff equations (see e.g. HAIRER and WANNER [27], IV.7). We assume $\gamma_{ii} = \gamma > 0$ for all i , which is the standard simplification to derive Rosenbrock methods with one and the same operator on the left-hand side of (17). The linearly implicit Euler method mentioned above is recovered for $s=1$ and $\gamma=1$.

For the general system

$$B(t, u) \partial_t u = f(t, u), \quad u(t_0) = u_0, \quad t > t_0, \quad (19)$$

an efficient implementation that avoids matrix-vector multiplications with the Jacobian was given by LUBICH and ROCHE [40]. In the case of a time- or solution-dependent matrix B , an approximation of $\partial_t u$ has to be taken into account, leading to the generalized Rosenbrock method of the form

$$\begin{aligned} \left(\frac{1}{\tau \gamma} B(t_n, u_n) - J_n \right) U_{ni} &= f(t_i, U_i) - B(t_n, u_n) \sum_{j=1}^{i-1} \frac{c_{ij}}{\tau} U_{nj} + \tau \gamma_i C_n \\ &+ (B(t_n, u_n) - B(t_i, U_i)) Z_i, \quad i = 1(1)s, \end{aligned} \quad (20)$$

where the internal values are given by

$$t_i = t_n + \alpha_i \tau, \quad U_i = u_n + \sum_{j=1}^{i-1} a_{ij} U_{nj}, \quad Z_i = (1 - \sigma_i) z_n + \sum_{j=1}^{i-1} \frac{s_{ij}}{\tau} U_{nj},$$

and the Jacobians are defined by

$$\begin{aligned} J_n &:= \partial_u (f(t, u) - B(t, u) z) |_{u=u_n, t=t_n, z=z_n}, \\ C_n &:= \partial_t (f(t, u) - B(t, u) z) |_{u=u_n, t=t_n, z=z_n}. \end{aligned}$$

This yields the new solution

$$u_{n+1} = u_n + \sum_{i=1}^s m_i U_{ni}$$

and an approximation of the temporal derivative $\partial_t u$

$$z_{n+1} = z_n + \sum_{i=1}^s m_i \left(\frac{1}{\tau} \sum_{j=1}^i (c_{ij} - s_{ij}) U_{nj} + (\sigma_i - 1) z_n \right) .$$

The new coefficients can be derived from α_{ij} , γ_{ij} , and b_i [40]. In the special case $B(t, u) = I$, we get (17) setting $U_{ni} = \tau \sum_{j=1, \dots, i} \gamma_{ij} K_{nj}$, $i = 1, \dots, s$.

Various Rosenbrock solvers have been constructed to integrate systems of the form (19). An important fact is that the formulation (19) includes problems of higher differential index. Thus, the coefficients of the Rosenbrock methods have to be specially designed to obtain a certain order of convergence. Otherwise, order reduction might happen. Among the Rosenbrock methods suitable for index 1 problems we mention ROS2 [15], ROS2POS[62], ROS3P [37], and RODAS4 [27]. More information can be found in [36]. These Rosenbrock solvers have been used in our simulations presented here.

Usually, one wishes to adapt the step size in order to control the temporal error. For linearly implicit methods of Rosenbrock type a second solution of inferior order, say \hat{p} , can be computed by a so-called embedded formula

$$\begin{aligned} \hat{u}_{n+1} &= u_n + \sum_{i=1}^s \hat{m}_i U_{ni} , \\ \hat{z}_{n+1} &= z_n + \sum_{i=1}^s \hat{m}_i \left(\frac{1}{\tau} \sum_{j=1}^i (c_{ij} - s_{ij}) U_{nj} + (\sigma_i - 1) z_n \right) , \end{aligned}$$

where the original weights m_i are simply replaced by \hat{m}_i . If p is the order of u_{n+1} , we call such a pair of formulas to be of order $p(\hat{p})$. Introducing an appropriate scaled norm $\|\cdot\|$, the local error estimator

$$r_{n+1} = \|u_{n+1} - \hat{u}_{n+1}\| + \|\tau(z_{n+1} - \hat{z}_{n+1})\| \quad (21)$$

can be used to propose a new time step by

$$\tau_{n+1} = \frac{\tau_n}{\tau_{n-1}} \left(\frac{TOL_t r_n}{r_{n+1} r_{n+1}} \right)^{1/(\hat{p}+1)} \tau_n . \quad (22)$$

Here, TOL_t is a desired tolerance prescribed by the user. This formula is related to a discrete PI-controller first established in the pioneering works of GUSTAFSSON, LUNDH, and SÖDERLIND [25, 24]. A more standard step size selection strategy can be found in HAIRER, NØRSETT, and WANNER ([26], II.4).

Rosenbrock methods offer several structural advantages. They preserve conservation properties like fully implicit methods. There is no problem to construct Rosenbrock methods with optimum linear stability properties for stiff equations. Because of their one-step nature, they allow a rapid change of step sizes and an efficient adaptation of the underlying spatial discretizations as will be seen in the next section. Thus, they are attractive for solving real world problems.

4.2 Multilevel finite elements

In the context of PDEs, system (20) consists of linear elliptic boundary value problems. In the spirit of spatial adaptivity a multilevel finite element method is used to solve this system. The main idea of the multilevel technique consists of replacing the solution space by a sequence of discrete spaces with successively increasing dimension to improve their approximation property. A posteriori error estimates provide the appropriate framework to determine where a mesh refinement is necessary and where degrees of freedom are no longer needed. Adaptive multilevel methods have proven to be a useful tool for drastically reducing the size of the arising linear algebraic systems and to achieve high and controlled accuracy of the spatial discretization (see e.g. BANK [5], DEUFLHARD, LEINEN, and YSERENTANT [19], LANG [35]).

Let T_h be an admissible finite element mesh at $t = t_n$ and S_h^q be the associated finite dimensional space consisting of all continuous functions which are polynomials of order q on each finite element $T \in T_h$. Then the standard Galerkin finite element approximation $U_{ni}^h \in S_h^q$ of the intermediate values U_{ni} satisfies the equation

$$(L_n U_{ni}^h, \phi) = (r_{ni}, \phi) \quad \text{for all } \phi \in S_h^q, \quad (23)$$

where L_n is the weak representation of the differential operator on the left-hand side in (20) and r_{ni} stands for the entire right-hand side in (20). Since the operator L_n is independent of i its calculation is required only once within each time step.

The linear systems are solved by direct or iterative methods. While direct methods work quite satisfactorily in one-dimensional and even two-dimensional applications, iterative solvers such as Krylov subspace methods perform considerably better with respect to CPU-time and memory requirements for large two- and three-dimensional problems. We mainly use the BICGSTAB-algorithm [63] with ILU-preconditioning.

After computing the approximate intermediate values U_{ni}^h a posteriori error estimates can be used to give specific assessment of the error distribution. Considering a hierarchical decomposition

$$S_h^{q+1} = S_h^q \oplus Z_h^{q+1}, \quad (24)$$

where Z_h^{q+1} is the subspace that corresponds to the span of all additional basis functions needed to extend the space S_h^q to higher order, an attractive idea of an efficient error estimation is to bound the spatial error by evaluating its components in the space Z_h^{q+1} only. This technique is known as hierarchical error estimation and has been accepted to provide efficient and reliable assessment of spatial errors (BORNEMANN, ERDMANN, and KORNHUBER [8], DEUFLHARD, LEINEN and YSERENTANT [19], BANK and SMITH [4]). In LANG [36], the hierarchical basis technique has been carried over to time-dependent nonlinear problems. Defining an a posteriori error estimator $E_{n+1}^h \in Z_h^{q+1}$ by

$$E_{n+1}^h = E_{n0}^h + \sum_{i=1}^s m_i E_{ni}^h \quad (25)$$

with E_{n0}^h approximating the projection error of the initial value u_n in Z_h^{q+1} and E_{ni}^h estimating the spatial error of the intermediate value U_{ni}^h , the local spatial error for a finite element $T \in T_h$ can be estimated by $\eta_T := \|E_{n+1}^h\|_T$. The error estimator E_{n+1}^h is computed by linear systems which can be derived from (23). For practical computations the spatially global calculation of E_{n+1}^h is normally approximated by a small element-by-element calculation. This leads to an efficient algorithm for computing a posteriori error estimates which can be used to determine an adaptive strategy to improve the accuracy of the numerical approximation where needed. A rigorous a posteriori error analysis for a Rosenbrock–Galerkin finite element method applied to nonlinear parabolic systems is given in LANG [36]. In our applications we applied linear finite elements and measured the spatial errors in the space of quadratic functions.

In order to produce a nearly optimal mesh, those finite elements T having an error η_T larger than a certain threshold are refined. After the refinement improved finite element solutions U_{ni}^h defined by (23) are computed. The whole procedure solve–estimate–refine is applied several times until a prescribed spatial tolerance $\|E_{n+1}^h\| \leq TOL_x$ is reached. To maintain the nesting property of the finite element subspaces coarsening takes place only after an accepted time step before starting the multilevel process at a new time. Regions of small errors are identified by their η -values.

5 Numerical simulations

Before proceeding, we show how the monodomain and the Bidomain model fit into the abstract setting (19)

$$B(t, u) \partial_t u = f(t, u), \quad u(t_0) = u_0, \quad t > t_0,$$

used above to describe time and spatial discretization.

We start with the monodomain model and set

$$\begin{aligned} B(t, u) &= \begin{pmatrix} c_m & 0 \\ 0 & I \end{pmatrix}, \\ f(t, u) &= \begin{pmatrix} I_{app} - I_{ion}(u) + \nabla \cdot (D_m \nabla u_1) \\ P(u) \end{pmatrix}, \end{aligned}$$

where

$$u = (v, w)^T, \quad I = 1, \quad P = \eta_2 \left(\frac{v}{v_p} - \eta_3 w \right),$$

for the FitzHugh-Nagumo variant and

$$\begin{aligned} u &= (v, h, j, m, d, f, X, [C_a]_i)^T, \quad I = \text{diag}(1, 1, 1, 1, 1, 1, 1), \\ P &= (R_1, \dots, R_7, S)^T, \quad R_k = \alpha_k(u_1)(1 - u_{k+1}) - \beta_k(u_1)u_{k+1}, \quad k = 1, \dots, 7 \\ S &= 0.07(10^{-4} - u_8) - 10^{-4}I_{si}(u) \end{aligned}$$

for the LR1 ion model. Here, u_k is the k -th component of the solution vector u . We note that the matrix B is regular.

For the Bidomain model, we have

$$\begin{aligned} B(t, u) &= \begin{pmatrix} c_m & -c_m & 0 \\ -c_m & c_m & 0 \\ 0 & 0 & I \end{pmatrix}, \\ f(t, u) &= \begin{pmatrix} -I_{ion} + \nabla \cdot (D_m \nabla u_1) \\ -I_{app} + I_{ion} + \nabla \cdot (D_m \nabla u_2) \\ P(u) \end{pmatrix}, \end{aligned}$$

where

$$u = (u_i, u_e, w)^T, \quad I = 1, \quad P = \eta_2 \left(\frac{v}{v_p} - \eta_3 w \right),$$

for the FitzHugh-Nagumo variant and

$$\begin{aligned} u &= (u_i, u_e, h, j, m, d, f, X, [C_a]_i)^T, v = u_1 - u_2, I = \text{diag}(1, 1, 1, 1, 1, 1, 1), \\ P &= (R_1, \dots, R_7, S)^T, \quad R_k = \alpha_k(v)(1 - u_{k+2}) - \beta_k(v)u_{k+2}, \quad k = 1, \dots, 7, \\ S &= 0.07(10^{-4} - u_9) - 10^{-4}I_{si}(v, u_3, \dots, u_9) \end{aligned}$$

for the LR1 ion model. Here, u_k is the k -th component of u . The matrix B is singular due to the upper 2×2 -matrix showing the differential-algebraic character of the Bidomain system (see also the equivalent formulation (3)). In all models, the Jacobians C_n and J_n reduce to $C_n = 0$ and $J_n = \partial_u f(u)|_{u=u_n}$.

Setting $u = (u_1, u_2, q)^T$ the nonlinear terms I_{ion} and P depend only on the difference $v = u_1 - u_2$, i.e., $I = I_{ion}(u_1 - u_2, q)$ and $P = P(u_1 - u_2, q)$. The operator matrix related to the problem (20) is given by

$$\mathcal{M} := \frac{1}{\tau\gamma} B(u) - J(u) = \begin{pmatrix} \frac{c_m}{\tau\gamma} - \nabla \cdot (D_i \nabla \cdot) + \partial_v I_{ion}(v, q) & -c_m \tau \gamma - \partial_v I_{ion}(v, q) & \partial_q I_{ion}(v, q) \\ -\frac{c_m}{\tau\gamma} - \partial_v I_{ion}(v, q) & \frac{c_m}{\tau\gamma} - \nabla \cdot (D_e \nabla \cdot) + \partial_v I_{ion}(v, q) & -\partial_q I_{ion}(v, q) \\ \partial_v P(v, q) & -\partial_v P(v, q) & \frac{I}{\tau\gamma} - \partial_q P(v, q) \end{pmatrix}$$

The vector $(\mu, \mu, 0)^T$, with μ constant, is the eigenfunction associated to the zero eigenvalue of B and \mathcal{M} as well. Therefore the solvability of the Bidomain problem is assured for right-hand sides that are orthogonal to this eigenfunction, i.e., $f(t, u) \cdot (\mu, \mu, 0) = 0$. It is easy to verify that for (20) the orthogonality condition holds if $\int_{\Omega} I_{app} dx = 0$, then the system admits a unique solution apart from an additive constant in the components u_i and u_e . The condition $\int_{\Omega} u_e dx = 0$ determines a solution and is enforced during each time step.

We have performed various simulations on a three-dimensional domain $\Omega = [1, 2] \times [1, 2] \times [1, 1.1]$ of size $1 \times 1 \times 0.1 \text{ cm}^3$, including both the Monodomain and the Bidomain model. Results are presented for the FHN-variant ionic model and the LR1 ionic model. The parameters used in our computations are given in Tab. 1. The fibers have constant direction and lie in the x-y plane (they are horizontal), forming a -45° angle with the x-axis.

The application that we study is a complete heartbeat in its three main phases at each point $\mathbf{x} \in \Omega$:

- (a) the excitation phase (depolarization), where the potential v undergoes an abrupt temporal change within 2 msec, followed by an exponential decay;

general	$\chi = 10^3 \text{ cm}^{-1}, C_m = 10^{-3} \text{ mF/cm}^2$
Monodomain	$\sigma_l = 1.2 \cdot 10^{-3} \Omega^{-1} \text{cm}^{-1}, \sigma_t = 2.5562 \cdot 10^{-4} \Omega^{-1} \text{cm}^{-1}$
Bidomain	$\sigma_l^e = 2 \cdot 10^{-3} \Omega^{-1} \text{cm}^{-1}, \sigma_l^i = 3 \cdot 10^{-3} \Omega^{-1} \text{cm}^{-1}$ $\sigma_t^e = 1.3514 \cdot 10^{-3} \Omega^{-1} \text{cm}^{-1}$ $\sigma_t^i = 3.1525 \cdot 10^{-4} \Omega^{-1} \text{cm}^{-1}$ $\sigma_n^e = \sigma_t^e / \mu_1, \sigma_n^i = \sigma_t^i / \mu_2$ $\mu_1 = \mu_2 = 1$ axial isotropic case $\mu_1 = 2, \mu_2 = 10$ orthotropic case
FHN-variant	$G = 1.5 \Omega^{-1} \text{cm}^{-2}, v_{th} = 13 \text{ mV}, v_p = 100 \text{ mV}$ $\eta_1 = 4.4 \Omega^{-1} \text{cm}^{-2}, \eta_2 = 0.012, \eta_3 = 1$
LR1	as in original paper [41] except G_{si} reduced by a factor 2/3

Table 1: Parameters calibration for numerical tests

- (b) the plateau phase lasting from 40-50 msec to about 400 msec according to the ionic model chosen and the type of propagating front considered; v varies very little and slowly compared to the excitation phase and the cardiac tissue is refractory, i.e., any applied stimulus does not elicit another action potential;
- (c) the recovery phase (repolarization), where v returns to the rest value during a period of 20-50 msec, after which the tissue becomes excitable again.

The excitation process is started by applying a stimulus of $200 \mu\text{A/cm}^3$ for 1 msec in a small area close to the center of the epicardium.

For all computations we use an initial coarse mesh consisting of 600 tetrahedral finite elements, see Figure 1. Our KARDOS code automatically adapts the spatial meshes and time steps in order to follow local phenomena of the whole heartbeat. While locally refined meshes and small time steps are chosen to accurately resolve the travelling excitation and repolarization fronts, coarse meshes and larger time steps are sufficient during the plateau phase.

Normally, we choose as tolerances for accuracy in time $TOL_t = 0.01$ and in space $TOL_x = 0.01$. This might lead to exceeding our memory resources because too many points are necessary to guarantee the required precision in space. Therefore, we allow mesh refinement only up to *depth* 3 (LR1 model) or 4 (FHN model). The parameter *depth* counts how often a tetrahedron

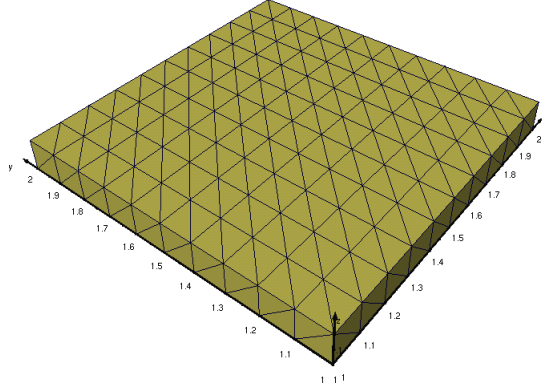


Figure 1: Initial mesh.

in the initial mesh is refined. Alternatively, we could restrict the maximum number of points in the grid.

5.1 Monodomain–FHN model

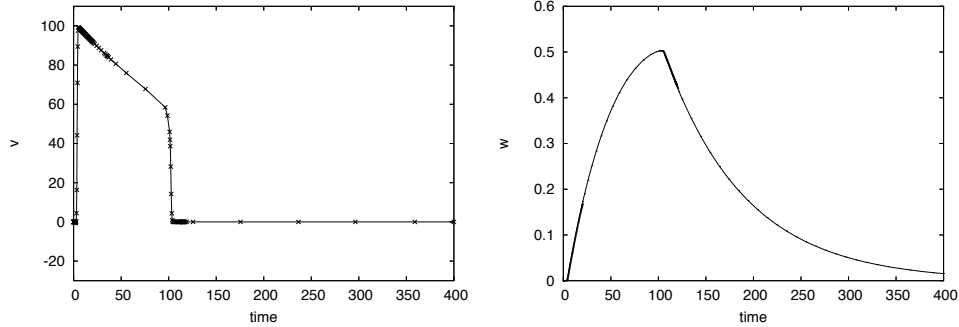


Figure 2: Monodomain–FHN model: potential v and gating variable w in point $(1.65, 1.65, 1.10)$ as a function of time. Time integrator: ROS3P.

Our first results for the Monodomain–FHN model are taken from a simulation with the time integrator ROS3P. We show in Figure 3 the evolution of the potential v and the corresponding adaptive meshes during propagation of the excitation front and the subsequent plateau phase. Typical profiles of the solution components observed in the spatial point $\mathbf{x} = (1.65, 1.65, 1.10)$ are presented in Figure 2. One can clearly see the exponential increase and decrease of the potential v between the phases that are numerically resolved

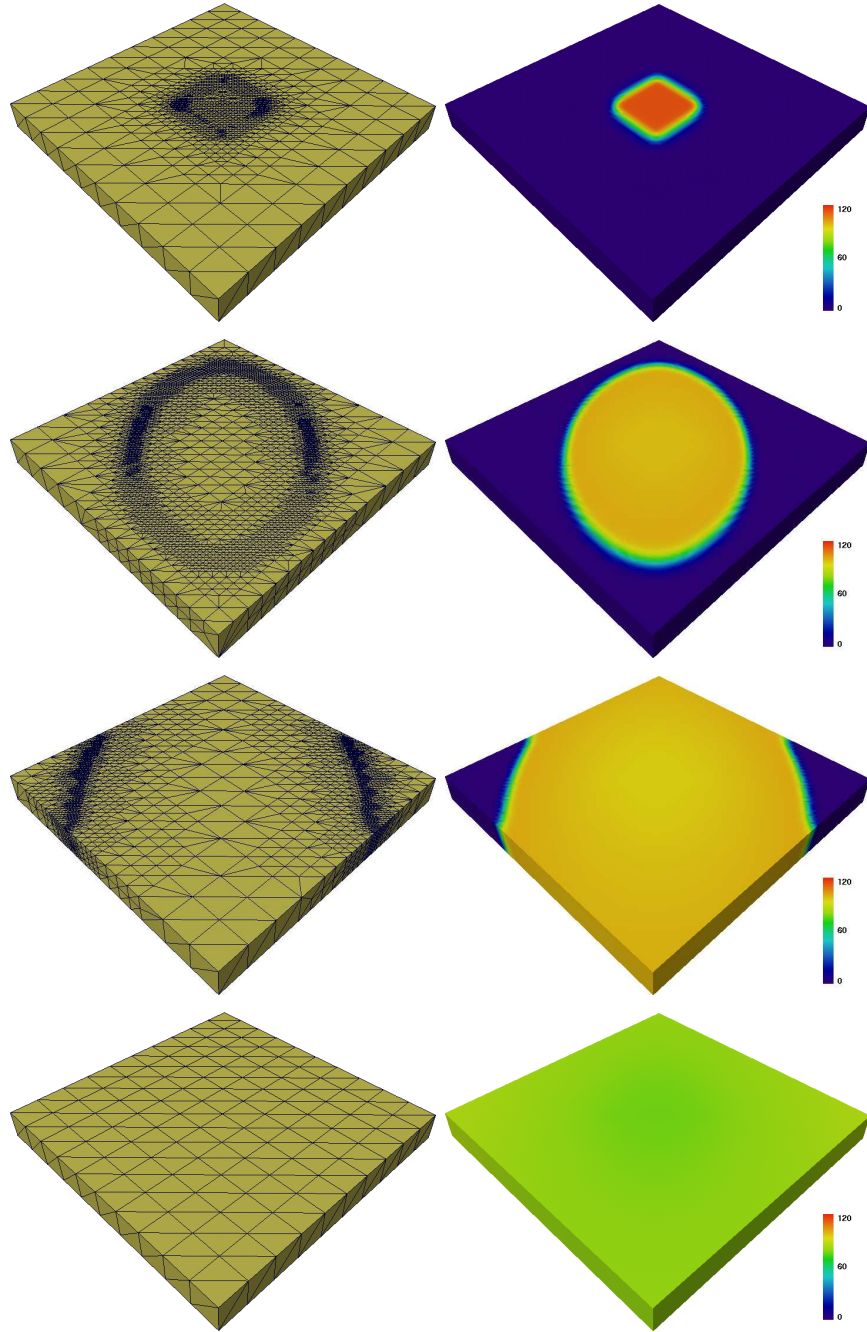


Figure 3: Monodomain–FHN model: mesh and potential v at times 1, 7, 13, 50 msec.

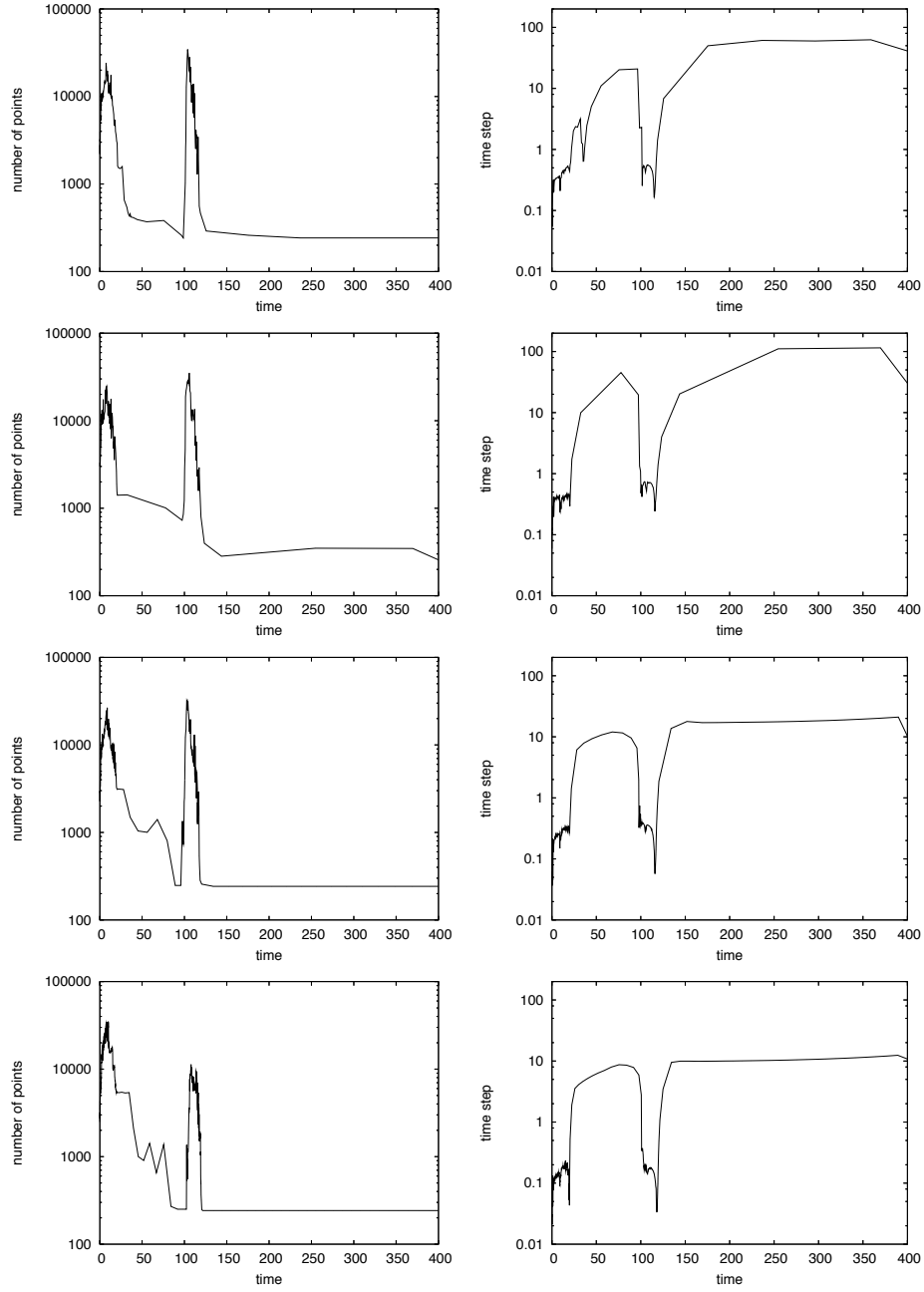


Figure 4: Monodomain-FHN model: number of vertices and time step size as functions of time for different time integrators: ROS3P (row 1), RODAS4 (row 2), ROS2POS (row 3), ROS2 (row 4).

by smaller time steps, see Figure 4 (right).

Next, we examine the performance of several Rosenbrock methods for the same tolerances TOL_t and TOL_x . We compare the number of grid points and the time steps chosen by the second-order methods ROS2 ($s = 2$ in (20)) and ROS2POS ($s = 3$ in (20)), the third-order method ROS3P ($s = 3$ in (20)) and the fourth-order method RODAS4 ($s = 6$ in (20)). All integrators select small time steps and finer grids for the transition between the phases, i.e., from excitation to plateau and from plateau to recovery, whereas elsewhere rather coarse grids and large time steps are chosen, see Figure 4. Due to their higher order ROS3P and RODAS4 select larger time steps than ROS2 and ROS2POS. RODAS4 reaches the final time in 108 steps, ROS3P needs 130 steps, ROS2POS 208 steps, and ROS2 even 360 steps. Though one step of ROS2 is much cheaper than one step of RODAS4, it takes twice as much computing time for the whole calculation. The best performance with respect to accuracy and computing time is obtained by ROS3P.

A closer look at the potential v at point $\mathbf{x} = (1.65, 1.65, 1.10)$ in the time interval $[90, 110]$ reveals that ROS2 produces a slower propagation of the recovery front compared to the other Rosenbrock solvers, Figure 6. The reason for this behavior is the insufficient resolution in space provided by ROS2 – a fact that can be seen from Figure 4, bottom left.

5.2 Monodomain–LR1 model

For the Monodomain–LR1 model, we have also compared various Rosenbrock integrators, and again ROS3P proved to be most efficient. Plots of the action potential v , gating variables w_1, \dots, w_6 , and calcium concentration w_7 in the point $(1.9, 1.9, 1.0)$ as a function of time are shown in Figure 5.

Small time steps are necessary only in the depolarization and repolarization phases; elsewhere the time step increases by two orders of magnitude. Similar observations can be made for the spatial resolution, see Figure 7.

In Figure 8, we present results for the action potential v and the gating variables w_1 and w_2 which are obtained for two different spatial tolerances. Whereas a less accurate resolution in space yields unphysical oscillations in all solution components, a more restrictive tolerance reduces this effect drastically.

5.3 Bidomain–FHN model

We used the Rosenbrock method ROS3P for integrating the Bidomain–FHN model. Plots of the intra- and extra-cellular electric potentials u_i ,

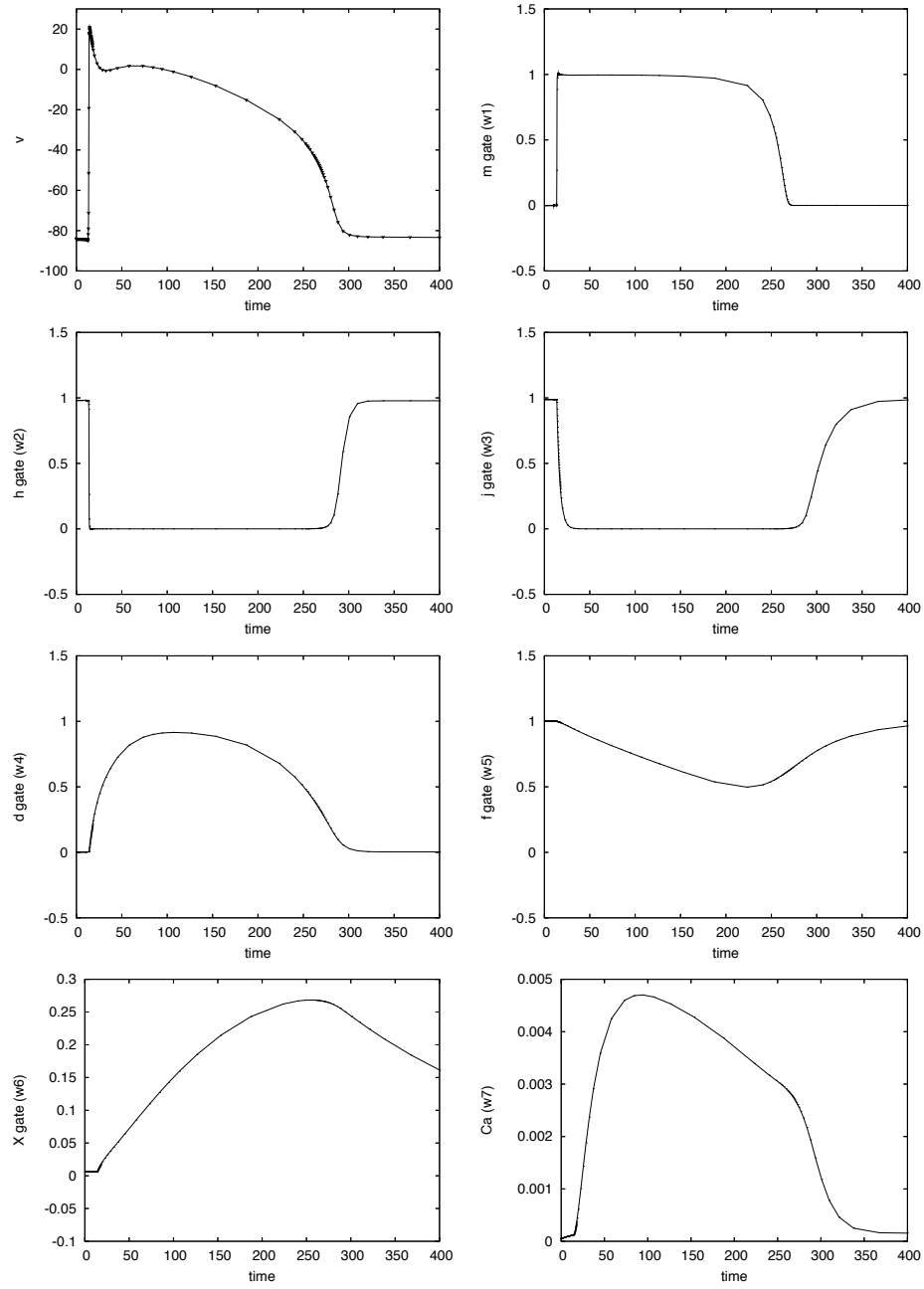


Figure 5: LR1 membrane model: action potential v , gating variables w_1 , ..., w_6 , calcium concentration w_7 in point (1.9,1.9,1.0) as a function of time. Time integrator: ROS3P

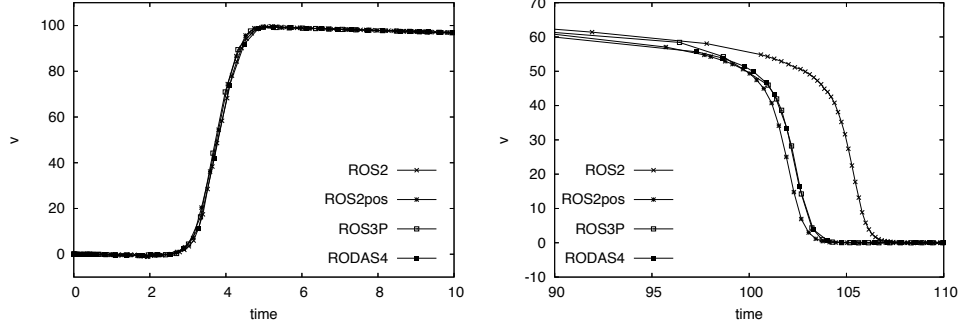


Figure 6: Monodomain-FHN model: excitation and recovery front of potential v at point $(1.65, 1.65, 1.10)$ as a function of time for different time integrators.

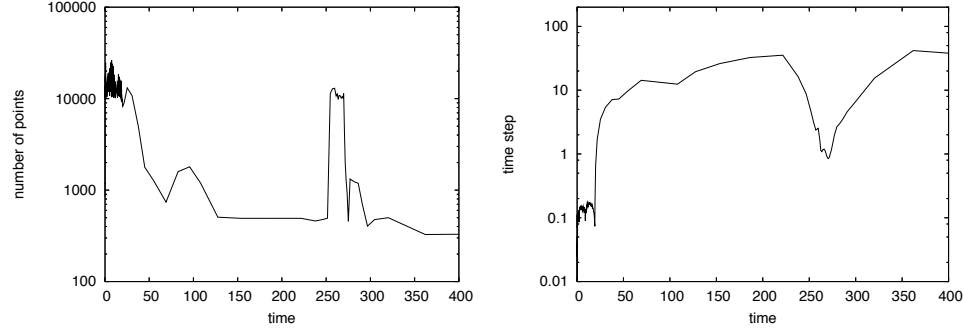


Figure 7: Monodomain-LR1 model: number of vertices and time step size as functions of time. Time integrator: ROS3P

u_e in two different points, $(1.65, 1.65, 1.1)$ and $(1.9, 1.9, 1.0)$, as a function of time are shown in Figure 9. We recognize that there is not only a front moving through the space, but much more dynamics. In particular, the extra-cellular potentials vary a lot depending on the point x , both in the first wave complex (the QRS) and the last little wave (the T wave). Figure 10 shows the behaviour of u_i and u_e in more detail for the first 20 msec. The development of the gating variable w is less complex, see Figure 11.

The evolution of the number of points and time steps are shown in Figure 12. The mechanism of local error control works as optimal as in the Monodomain models.

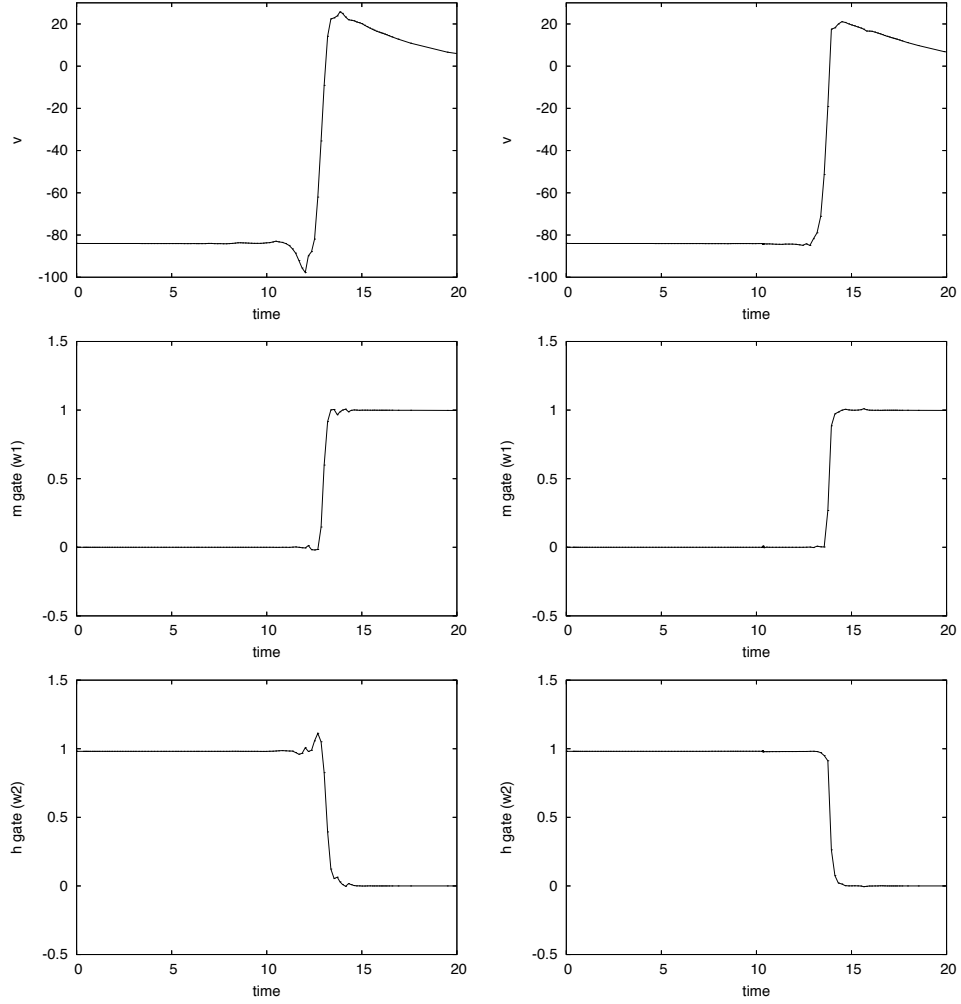


Figure 8: LR1 membrane model: action potential v , gating variables w_1 , w_2 in point $(1.9, 1.9, 1.0)$ as a function of time, computed with spatial accuracy $TOL_x = 0.01$ (left column) or $TOL_x = 0.001$ (right column). Time integrator: ROS3P

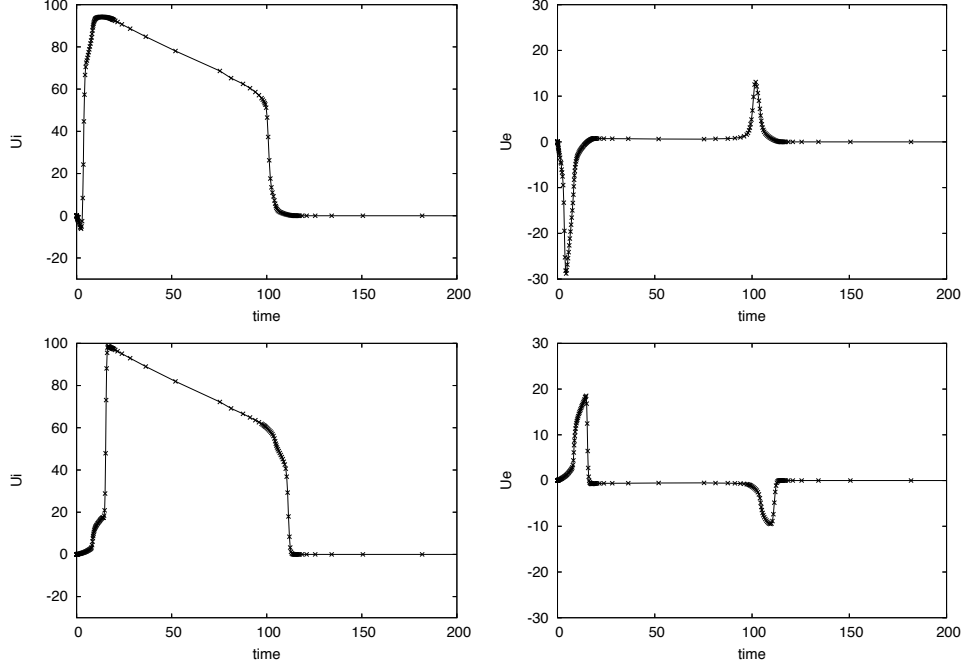


Figure 9: Bidomain–FHN model: intra- and extra-cellular electric potentials u_i , u_e in point (1.65,1.65,1.1) (top row) and in point (1.9,1.9,1.0) (bottom row) as a function of time. Time integrator: ROS3P.

5.4 Bidomain–LR1 model

Even in the most complex example of Bidomain–LR1 model the adaptive strategy of the code KARDOS works properly. Here we present results from calculations based on the time discretizations ROS3P and RODAS4. Figure 13 shows the extra- and intra-cellular electric potentials u_e and u_i over the whole period of 400 msec.

The detailed behaviour of u_e and u_i in the excitation phase can be seen in Figure 14. Here and in the transient phase between plateau and repolarization phase we need fine grids and small time steps, but elsewhere we save computer resources by large time steps and coarse grids, compare Figure 15 for method ROS3P and Figure 16 for RODAS4.

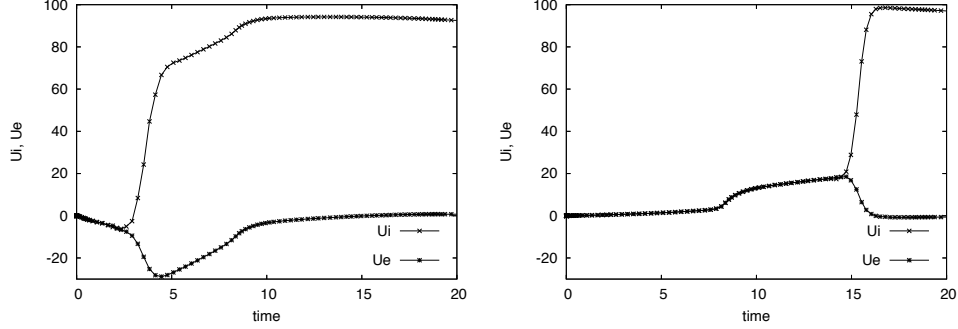


Figure 10: Bidomain–FHN model: intra- and extra-cellular electric potentials u_i , u_e in point (1.65,1.65,1.1) (left) and in point (1.9,1.9,1.0) (right) in the first 20 msec. Time integrator: ROS3P.

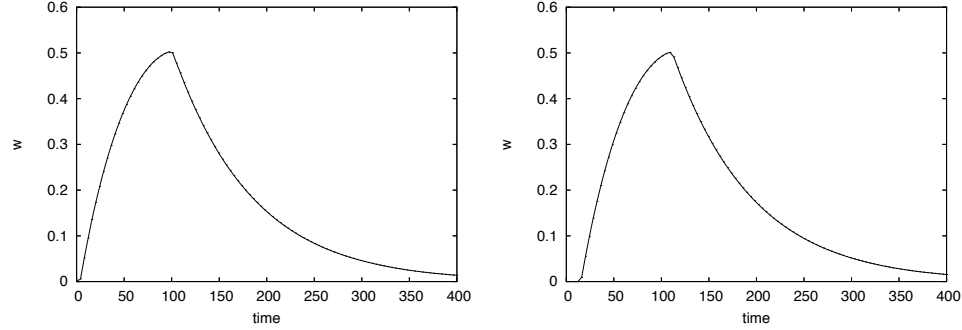


Figure 11: Bidomain–FHN model: gating variable w in point (1.65,1.65,1.1) (left) and in point (1.9,1.9,1.0) (right) as a function of time. Time integrator: ROS3P.

6 Conclusions and Outlook

We have presented a fully adaptive approach to solve various three-dimensional reaction–diffusion models arising in computational electrophysiology. The model complexity ranges from a simple Monodomain–FHN model to a more complex Bidomain–LR1 model. Due to steep solution gradients and travelling fronts an appropriate local adaptation of spatial and temporal discretizations in an automatic way turns out to be an important issue not only to maintain computer resources but also to get accurate solutions.

We have compared several linearly implicit one–step methods of

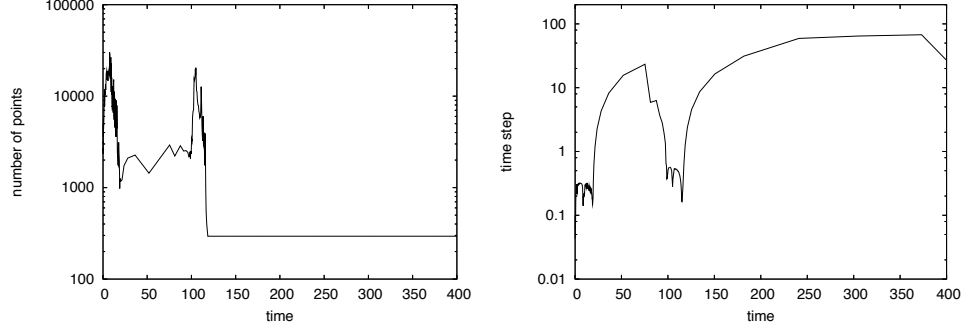


Figure 12: Bidomain-FHN model: number of vertices and time step size as functions of time. Time integrator: ROS3P

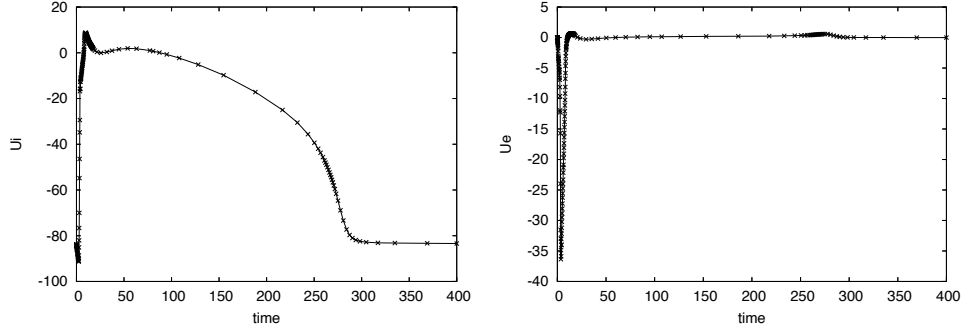


Figure 13: Bidomain-LR1 model: intra- and extra-cellular electric potentials u_i , u_e in point (1.65,1.65,1.1) as a function of time. Time integrator: ROS3P.

Rosenbrock-type. The three-stage third-order method ROS3P performed best.

Future work will focus on more general computational domains. Moreover, we are planning to compare the efficiency of the method presented here with the parallel solver of COLLI FRANZONE and PAVARINO, [13, 14].

7 Acknowledgement

We want to thank Rainer Roitzsch, Zuse Institute Berlin, who provided a lot of ideas to improve the code and the layout of the paper. We also are grateful for fruitful discussions with Ulrich Nowak, Zuse Institute Berlin, about stable integration of the LUO-RUDY ionic model.

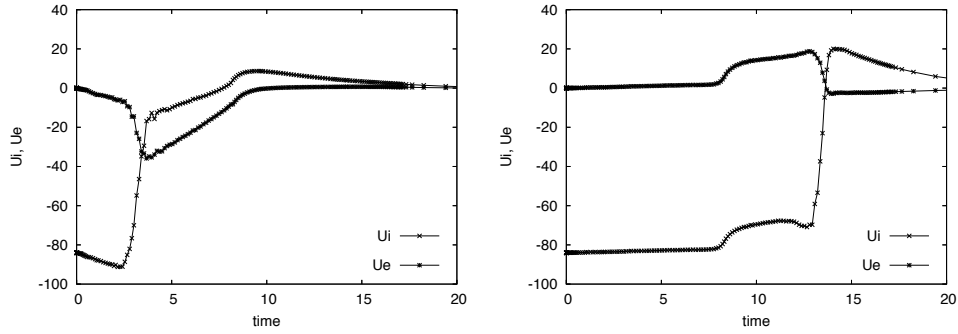


Figure 14: Bidomain-LR1 model: excitation phase of intra- and extra-cellular electric potentials u_i , u_e in point (1.65,1.65,1.1) (left) and in point (1.9,1.9,1.0) (right) in the first 20 msec. Time integrator: ROS3P.

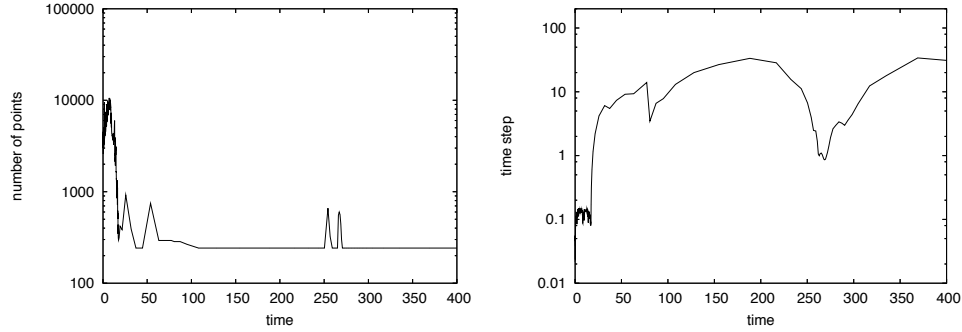


Figure 15: Bidomain-LR1 model: number of vertices and time step size as functions of time. Time integrator: ROS3P.

All visualizations in this paper have been created using AMIRA – a system for advanced visual data analysis, see [2, 56].

References

- [1] <http://www.zib.de/Numerik/numsoft/kardos>
- [2] <http://amira.zib.de/>
- [3] T. Ashihara, T. Namba, M. Ito, T. Ikeda, K. Nakazawa and N. Trayanova, Spiral wave control by a localized stimulus: A bidomain model study, *J. Cardiovasc. Electr.* 15 (2): 226–233, 2004.

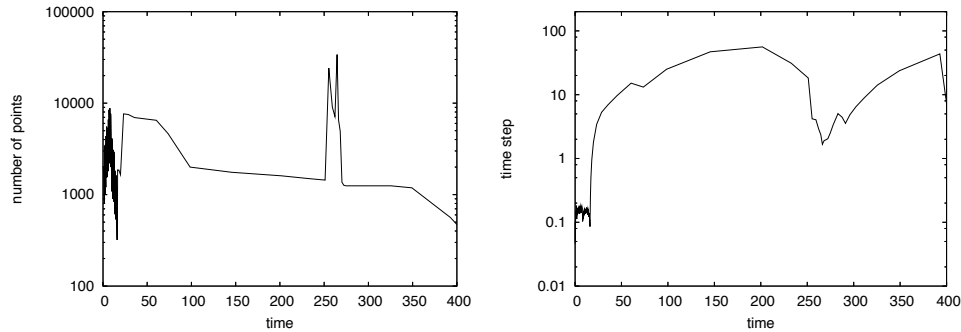


Figure 16: Bidomain-LR1 model: number of vertices and time step size as functions of time. Time integrator: RODAS4.

- [4] R.E. Bank and R.K. Smith, A Posteriori Error Estimates Based on Hierarchical Bases, *SIAM J. Numer. Anal.* **30** (1993), 921–935.
- [5] R.E. Bank, PLTMG: A Software Package for Solving Elliptic Partial Differential Equations - User's Guide 8.0, *SIAM*, 1998.
- [6] F.A. Bornemann, An Adaptive Multilevel Approach to Parabolic Equations. II. Variable-Order Time Discretization Based on a Multiplicative Error Correction, *IMPACT of Comput. in Sci. and Engrg.* **3** (1991), 93–122.
- [7] F.A. Bornemann, An Adaptive Multilevel Approach to Parabolic Equations. III. 2D Error Estimation and Multilevel Preconditioning, *IMPACT of Comput. in Sci. and Engrg.* **4** (1992), 1–45.
- [8] F.A. Bornemann, B. Erdmann, and R.Kornhuber, A Posteriori Error Estimates for Elliptic Problems in Two and Three Space Dimensions, *SIAM J. Numer. Anal.* **33** (1996), 1188–1204.
- [9] E. M. Cherry, H. S. Greenside and C. S. Henriquez, A space-time adaptive method for simulating complex cardiac dynamics, *Phys. Rev. Lett.* **84** (6): 1343-1346, 2000.
- [10] P. Colli Franzone, L. Guerri, and S. Roveda, Wavefront propagation in an activation model of the anisotropic cardiac tissue: Asymptotic analysis and numerical simulations, *J. Math. Biol.*, **28**, 121–176, 1990.

- [11] P. Colli Franzone, L. Guerri, Spread of excitation in 3-D models of the anisotropic cardiac tissue, I. Validation of the eikonal approach, *Math. Biosci.* **113** (1993), 145-209.
- [12] P. Colli Franzone and G. Savaré, Degenerate evolution systems modeling the cardiac electric field at micro and macroscopic level. In *Evolution equations, Semigroups and Functional Analysis*, A. Lorenzi and B. Ruf, Editors, 49–78, Birkhauser, 2002.
- [13] P. Colli Franzone and L. F. Pavarino, A parallel solver for reaction-diffusion systems in computational electrocardiology, *Math. Mod. Meth. Appl. Sci.* 14 (6): 883–911, 2004.
- [14] P. Colli Franzone, L. F. Pavarino, and B. Taccardi, Simulating patterns of excitation, repolarization and action potential duration with cardiac Bidomain and Monodomain models, *Math. Biosci.*, 2005, to appear.
- [15] K. Dekker and J.G. Verwer, Stability of Runge–Kutta methods for stiff nonlinear differential equations, *North–Holland Elsevier Science Publishers*, 1984.
- [16] P. Deuffhard, Uniqueness Theorems for Stiff ODE Initial Value Problems, in: *D.F. Griffiths and G.A. Watson (eds.), Numerical Analysis 1989, Proceedings of the 13th Dundee Conference, Pitman Research Notes in Mathematics Series 228, Longman Scientific and Technical* (1990), 74–87.
- [17] P. Deuffhard, Recent Progress in Extrapolation Methods for Ordinary Differential Equations, *SIAM Rev.* **27** (1985), 505–535.
- [18] P. Deuffhard and F. Bornemann, Numerische Mathematik II, Integration Gewöhnlicher Differentialgleichungen, *De Gruyter Lehrbuch, Berlin, New York*, 1994.
- [19] P. Deuffhard, P. Leinen, and H. Yserentant, Concepts of an Adaptive Hierarchical Finite Element Code, *IMPACT of Comput. in Sci. and Engrg.* **1** (1989), 3–35.
- [20] P. Deuffhard, J. Lang, and U. Nowak, Adaptive Algorithms in Dynamical Process Simulation, in: *H. Neunzert (ed.), Progress in Industrial Mathematics at ECMI'94, Wiley–Teubner* (1996), 122–137.
- [21] B. Erdmann, J. Lang, R. Roitzsch, KARDOS User's Guide. Technical Report ZR-02-42, Konrad-Zuse-Zentrum Berlin (ZIB), 2002.

- [22] B. Erdmann, J. Lang, and R. Roitzsch, KASKADE Manual, Version 2.0, Report TR93-5, Konrad-Zuse-Zentrum Berlin (ZIB), 1993.
- [23] L.P. Franca and S.L. Frey, Stabilized Finite Element Methods, *Comput. Methods Appl. Mech. Engrg.* **99** (1992), 209–233.
- [24] K. Gustafsson, Control-Theoretic Techniques for Step Size Selection in Implicit Runge-Kutta Methods, *ACM Trans. Math. Software* **20** (1994), 496–517.
- [25] K. Gustafsson, M. Lundh, and G. Söderlind, A PI Step Size Control for the Numerical Solution of Ordinary Differential Equations, *BIT* **28** (1988), 270–287.
- [26] E. Hairer, S.P. Nørsett, and G. Wanner, Solving Ordinary Differential Equations I, Nonstiff Problems, *Springer-Verlag, Berlin, Heidelberg, New York*, 1987.
- [27] E. Hairer and G. Wanner, Solving Ordinary Differential Equations II, Stiff and Differential-Algebraic Problems, *Second Revised Edition*, *Springer-Verlag, Berlin, Heidelberg, New York*, 1996.
- [28] C. S. Henriquez, Simulating the electrical behavior of cardiac tissue using the bidomain model, *Crit. Rev. Biomed. Eng.* 21: 1–77, 1993.
- [29] C. S. Henriquez, A. L. Muzikant and C. K. Smoak, Anisotropy, fiber curvature, and bath loading effects on activation in thin and thick cardiac tissue preparations: Simulations in a three-dimensional bidomain model, *J. Cardiovasc. Electrophysiol.* 7 (5): 424–444, 1996.
- [30] A. L. Hodgkin and A. F. Huxley, A quantitative description of membrane current and its application to conduction and excitation in nerve, *J. Physiol.*, 117:500–544, 1952.
- [31] N. Hooke, C. S. Henriquez, P. Lanzkrom, and D. Rose, Linear algebraic transformations of the bidomain equations: implications for numerical methods, *Math. Biosc.* 120:127–145, 1994.
- [32] T. J. Hund and Y. Rudy, Rate transient and regulation of action potential and calcium transient in a canine cardiac ventricular cell model, *Circulation* 110:3168–3174, 2004.
- [33] J. P. Keener and J. Sneyd. *Mathematical Physiology*. Springer-Verlag, New York 1998.

- [34] A. G. Kleber and Y. Rudy, Basic mechanisms of cardiac impulse propagation and associated arrhythmias, *Physiol. Rev.* 84 (2): 431–488, 2004.
- [35] J. Lang, Adaptive FEM for Reaction–Diffusion Equations, *Appl. Numer. Math.* **26** (1998), 105–116.
- [36] J. Lang. *Adaptive Multilevel Solution of Nonlinear Parabolic PDE Systems. Theory, Algorithm, and Applications*. LNCSE vol. 16, Springer-Verlag, 2000.
- [37] J. Lang and J. Verwer, ROS3P - an Accurate Third–Order Rosenbrock Solver Designed for Parabolic Problems, *Report MAS-R0013*, CWI, Amsterdam, 2000.
- [38] J. Lang and A. Walter, A Finite Element Method Adaptive in Space and Time for Nonlinear Reaction–Diffusion Systems, *IMPACT of Comput. in Sci. and Engrg.* **4** (1992), 269–314.
- [39] I. J. LeGrice, B. H. Smaill and P.J. Hunter, Laminar structure of the heart: a mathematical model, *Am. J. Physiol. (Heart Circ. Physiol.)*, 272 (41): H2466–H2476, 1997.
- [40] Ch. Lubich and M. Roche, Rosenbrock Methods for Differential–Algebraic Systems with Solution–Dependent Singular Matrix Multiplying the Derivative, *Comput.* **43**, 325–342, (1990).
- [41] C. Luo and Y. Rudy, A model of the ventricular cardiac action potential: depolarization, repolarization, and their interaction, *Circ. Res.* 68 (6): 1501–1526, 1991.
- [42] P. K. Moore, An adaptive finite element method for parabolic differential systems: some algorithmic considerations in solving in three space dimensions, *SIAM J. Sci. Comput.* 21 (4): 1567–1586, 2000.
- [43] M. Murillo and X.C. Cai, A fully implicit parallel algorithm for simulating the non-linear electrical activity of the heart, *Numer. Linear Algebra* 11 (2-3): 261–277, 2004.
- [44] A. Muzikant, E. W. Hsu, P. D. Wolf and C. S. Henriquez, Region specific modeling of cardiac muscle: comparison of simulated and experimental potentials, *Ann. Biomed. Eng.* 30: 867–883, 2003.
- [45] A. V. Panfilov and A. V. Holden. *Computational Biology of the Heart*. Wiley, 1997.

- [46] L. F. Pavarino and P. Colli Franzone, Parallel solution of cardiac reaction-diffusion models. In *Domain Decomposition Methods in Science and Engineering*, Kornhuber et al. (Eds.), LNCSE vol. 40: 669–676, Springer, 2004.
- [47] M. Pennacchio and V. Simoncini, Efficient algebraic solution of reaction-diffusion systems for the cardiac excitation process, *J. Comput. Appl. Math.* 145 (1): 49–70, 2002.
- [48] J. Pormann, A Simulation System for the Bidomain Equations. P. D. Thesis, Duke Univ., Dept. of Electr. Comput. Eng., 1999.
- [49] M. Roche, Runge–Kutta and Rosenbrock Methods for Differential–Algebraic Equations and Stiff ODEs, *PhD thesis, Université de Genève*, 1988.
- [50] J. M. Rogers and A. D. McCulloch, A collocation-Galerkin finite element model of cardiac action potential propagation, *IEEE Trans. Biomed. Eng.* 41: 743–757, 1994.
- [51] H.H. Rosenbrock, Some General Implicit Processes for the Numerical Solution of Differential Equations, *Computer J.* (1963), 329–331.
- [52] B. J. Roth, Action potential propagation in a thick strand of cardiac muscle, *Circ. Res.* 68: 162–173, 1991.
- [53] B. J. Roth, How the anisotropy of the intracellular and extracellular conductivities influence stimulation of cardiac muscle, *J. Math. Biol.* 30: 633–646, 1992.
- [54] B. J. Roth, Meandering of spiral waves in anisotropic cardiac tissue, *Physica D*, 150 (1-2): 127–136, 2001.
- [55] A. Sambelashvili and I. R. Efimov, Dynamics of virtual electrode-induced scroll-wave reentry in a 3D bidomain model, *Am. J. Physiol. Heart C.* 287 (4): 1570–1581, 2004.
- [56] D. Stalling, M. Westerhoff, H.-C. Hege, Amira: A Highly Interactive System for Visual Data Analysis, in: Charles D. Hansen, Christopher R. Johnson (eds.), *The Visualization Handbook*, Chapter 38, pp. 749–767 Elsevier, 2005.
- [57] K. Strehmel and R. Weiner, Linear–implizite Runge–Kutta–Methoden und ihre Anwendungen, *Teubner Texte zur Mathematik 127*, Teubner Stuttgart, Leipzig, 1992.

- [58] J. Sundnes, G. T. Lines, P. Grottnum and A. Tveito, Electrical activity in the human heart, in *Advanced Topics in Computational Partial Differential Equations*. H.P. Langtangen and A. Tveito eds., LNCSE vol. 33, Ch. 10: 401–449, Springer 2004.
- [59] D. Streeter, Gross morphology and fiber geometry in the heart, in *Handbook of Physiology*. Vol. 1, Sect. 2, pp. 61-112. R. M. Berne, Editor, Williams & Wilkins, 1979.
- [60] L. Tobiska and R. Verfürth, Analysis of a Streamline Diffusion Finite Element Method for the Stokes and Navier–Stokes Equation, *SIAM J. Numer. Anal.* **33** (1996), 107–127.
- [61] J. A. Trangenstein and C. Kim, Operator Splitting and Adaptive Mesh Refinement for the Luo-Rudy I Model, *J. Computational Physics* **196** (2004), 645–679, Elsevier.
- [62] J. G. Verwer, E. J. Spee, J. G. Blom, W. Hundsdorfer, A second-order Rosenbrock method applied to photochemical dispersion problems, *SIAM J. Sci. Comput.* **20** (4) (2002), 1456–1480.
- [63] H.A. van der Vorst, BI–CGSTAB: A fast and smoothly converging variant of BI–CG for the solution of nonsymmetric linear systems, *SIAM J. Sci. Stat.* **13** (1992), 631–644.
- [64] E. J. Vigmond, F. Aguel and N. A. Trayanova, Computational techniques for solving the bidomain equations in three dimensions, *IEEE Trans. Biomed. Eng.* 49 (11): 1260–1269, 2002.
- [65] R. Weber Dos Santos, G. Plank, S. Bauer and E. J. Vigmond, Preconditioning techniques for the Bidomain equations. In *Domain Decomposition Methods in Science and Engineering*, Kornhuber et al. (Eds.), LNCSE vol. 40, Springer, 2004.
- [66] H. Yu, A local space-time adaptive scheme in solving two-dimensional parabolic problems based on domain decomposition methods, *SIAM J. Sci. Comput.* 23 (1): 304–322, 2001.
- [67] D. Zipes and J. Jalife. *Cardiac Electrophysiology*. 4th ed., W. B. Saunders Co., Philadelphia, 2004.